第 19 卷 第 2 期 (专辑)　　天 文 学 进 展　　Vol.19, No.2 (S.I.)
2001 年 6 月　　PROGRESS IN ASTRONOMY　　Jun., 2001

类 Crab 脉冲星的三维磁层外隙模型

郑广生[1]　　张　力[1,2]

(1. 香港大学物理系　香港)
(2. 云南大学物理系　昆明　650091)

摘　　要

利用三维脉冲星磁层模型研究了磁层外隙的几何结构. 首先用自洽模型确定"外隙"的垂直尺度, 在该模型中外隙尺度受回流的外隙流 (带有隙加速的带电粒子发射的曲率光子) 加热极帽而产生的热光子的碰撞而成对生成所限. 外隙的横向尺度也受本地对生成所限. 在脉冲星的磁层中, 原则上有两个拓扑分离的外隙, 允许同时进入和流出粒子. 不过, 流入粒子流产生的辐射形态受隙中本地对生成和恒星附近的磁对生成的严格的制约. 根据外隙及其本地结构的三维模型计算了类 Crab 脉冲星的辐射形态和相位分解谱.

关 键 词　γ 射线: 理论 — 脉冲星: 一般 — 恒星: 中子星 — 恒星: 辐射

分 类 号　P145.6

A Three-dimensional Outer-magnetospheric Gap Model for Crab-like Pulsars

Cheng K S[1]　　Zhang L[1,2]

([1] *Department of Physics, the University of Hong Kong*)
([2] *Department of Physics, Yunnan University, Kunming 650091)*

Abstract

We use a three dimensional pulsar magnetosphere model to study the geometry of outer-magnetospheric gaps. The vertical size of the "outer gap" is first determined by a self-consistent model in which the outer gap size is limited by pair production from collisions of thermal photons produced from polar cap heating by backflow outer gap current with curvature photons emitted by gap accelerated charged particles. The transverse size of the outer gap is also determined by local pair production limits. In principle, there are two topologically disconnected outer gaps in the magnetosphere of a pulsar. Both incoming and outgoing particle flows are allowed. However, the emission morphologies produced by incoming particle flow is severely restricted

2000-12-27 收到

by local pair production in the gap and the absorption of magnetic pair production near the star. From the three dimensional structure of the outer gap and its local properties, we calculate the emission morphologies and phase-resolved spectra of Crab-like pulsars.

Key words gamma rays: theory—pulsars: general—stars: neutron—stars: radiation

1 Introduction

It has been argued that powerful acceleration regions, called "outer gaps", can form in the vicinity of "null charge surface" ($\mathbf{\Omega}\cdot\mathbf{B} = 0$) (Holloway 1973; Cheng, Ruderman & Sutherland 1976) because the charged carriers on each side of the null charge surface have opposite charges. Current passing through this surface removes charges in the vicinity of the null surface and a vacuum will form there. Cheng, Ho and Ruderman (1986) used an outer gap to calculate the phase-averaged spectrum of the Crab pulsar. Their model assumed that the radiation regions are thin in the longitudinal direction. Their double peak γ-ray structure was from two topologically disconnected outer gaps, each of which is associated with different magnetic poles. However, Romani and his co-workers (Chiang & Romani, 1992,1994; Romani and Yadigaroglu 1995; Romani 1996) have shown that *only one* outer gap with only outgoing current can produce a double-peak γ-ray light curve in a three-dimensional outer-magnetosphere. Using either a static dipolar field or a rotating dipolar field (results did not differ qualitatively) plus effects of time travel and aberration, they showed that an assumed outgoing current alone could produce a broad, irregularly-shaped emission beam which is particularly dense near the edge, so that two γ-ray peaks would be observed when the line of sight from the Earth crosses these enhanced γ-ray beam regions; the inner region of the beam provides a significant amount of emission between the peaks. EGRET has accumulated enough photons for Crab, Vela, PSR B1706-44 and Geminga to analyze the phase-resolved emission characteristics such as pulsed profiles and phase-resolved spectra (Fierro 1995; Thomson *et al.* 1996; Fierro *et al.* 1998). These data can give very strong constraint on theoretical models.

We re-consider the three dimensional magnetosphere, following the important ground-breaking work of Romani and co-workers. But instead of assuming a single outer gap with only an outgoing current, and no restriction on azimuthal directions, we use various physical processes (including pair production which depends sensitively on the local electric field and the local radius of curvature, surface field structure, reflection of $e^{\pm}$ pairs because of mirroring and resonant scattering) to determine the three-dimensional geometry of the outer gap. In our model, two outer gaps and both outgoing and incoming currents are in principle allowed, but it turns out that outgoing currents dominate the emitted radiation intensities.

2 The Model

2.1 Pair production and the structure of outer gaps

According to Cheng, Ruderman & Zhang (2000), we propose a structure of outer gaps determined by pair production conditions. The potential drop of the gap

$$\Delta V \approx 6.6 \times 10^{12} f_0^2 B_{12} P^{-2} \qquad \text{Volts}, \tag{1}$$

where $f_0 = h(< r >)/R_{\rm L}$, $h(< r >)$ is the average vertical separation of the gap boundaries in the (Ω, μ) plane and $R_{\rm L} = c/\Omega$ is the light cylinder radius, and $< r >$ is the average distance to the gap; its value depends on magnetic inclination angle χ ($< r > \approx R_{\rm L}/2$). The particle current passing through the gap is

$$\dot{N}_{\rm gap} = 3 \times 10^{30} f_0 \xi B_{12} P^{-2} \quad {\rm s}^{-1} \tag{2}$$

where $\xi = \Delta\Phi/2\pi$; $\Delta\Phi$ is the transverse (ϕ-direction) extension of the gap. Each of the charged particles inside the gap will radiate high-energy curvature photons with a characteristic energy

$$E_\gamma(f_0) = 2 \times 10^8 f_0^{3/2} B_{12}^{3/4} P^{-7/4} \qquad \text{eV}. \tag{3}$$

About half of $\dot{N}_{\rm gap}$ will move toward the star. Although they continue to radiate their energies on the way to the star, they still carry $10.5P^{1/3}$ ergs of energy on to the stellar surface. The energy will be radiated back out in hard X-rays. However, resonant scattering with pairs near the star may reflect hard X-rays back to the stellar surface (Cheng, Gil & Zhang 1998; Wang *et al.* 1998), to be re-emitted as soft X-rays with a temperature

$$T_{\rm s} \approx 3.8 \times 10^6 f_0^{1/4} \xi^{1/4} B_{12}^{1/2} P^{-5/12} \qquad \text{K}. \tag{4}$$

The X-ray photon density is very low but each pair produced by an X-ray-curvature photon collisions in the outer gap will emit almost 10^5 curvature γ-rays for further pair creation in that gap. Once the pair production threshold condition $kT_{\rm s}E_\gamma \geq (m_{\rm e}c^2)^2$ is satisfied, the gap is unlikely to grow much larger. This pair production condition gives

$$f_0 = 5.5 P^{26/21} B_{12}^{-4/7} \xi^{1/7}. \tag{5}$$

Here, ξ is still an unknown quantity. However, we see that f_0 is weakly dependent on ξ which is likely on the order of unity. In first approximation, we assume $f_0 = 5.5P^{26/21}B_{12}^{-4/7}$ (Zhang & Cheng 1997). To determine ξ, we need to consider local pair production processes. The pair production per unit length inside the gap is a decreasing function of r. According to Cheng, Ho and Ruderman (1986), $E_{||} \propto r^{-1/2}$ for the thin outer gap (e.g. the Crab pulsar), which gives $E_\gamma(r) \propto r^{-1/8}$ after using the large r limit $s(r) = (rR_L)^{1/2}$. Since E_γ is only weakly dependent on r, we assume $\sigma_{\gamma\gamma} \approx const.$.

The local pair production per unit length is

$$N_{\rm e^\pm}(r) = (1 - {\rm e}^{-\tau_{\gamma\gamma}}) N_\gamma(r) \approx \tau_{\gamma\gamma} N_\gamma(r), \tag{6}$$

where $\tau_{\gamma\gamma} = n_{\rm X}(r)\sigma_{\gamma\gamma}l(r)$ is the local optical depth, $n_{\rm X} = R^2T_{\rm s}^4\sigma/r^2kT_{\rm s}c$ is the X-ray number density at r, $l(r) \approx (2s(r)f(r)R_{\rm L})^{1/2}$ is the local optical path, $f(r) = h(r)/R_{\rm L}$ is the local vertical extension of the gap (since $B(r)h^2(r)$ is a constant, which gives $f(r) \propto r^{3/2}$ and $f_0 \approx f(R_L/2)$, and $N_\gamma = eE_{||}(r)/E_\gamma(r)$ is the number of curvature photons emitted at r per e^+/e^- per unit length. Then

$$N_{\rm e\pm}(r) \propto r^{-11/8}. \tag{7}$$

We see that most pairs are produced near the null surface where $r = r_{\rm in}$. We estimate that the pair production will take place mainly in the range $r_{\rm in} \leq r \leq r_{\rm lim}$ where $r_{\rm lim}$ is estimated as $r_{\rm lim}N_{\rm e\pm}(r_{\rm lim})/r_{\rm in}N_{\rm e\pm}(r_{\rm in}) \approx (r_{\rm lim}/r_{\rm in})^{-3/8} \approx 1/2$, which gives $r_{\rm lim} \approx 6r_{\rm in}$. This limits pair production both along the field lines and in transverse directions, and gives

$$\Delta\Phi \approx 160^\circ. \tag{8}$$

Within the pair production regions, outgoing and incoming directions for particle flows are allowed. For $r > r_{\rm lim}$ only outgoing current is possible.

Polar cap shape defines the boundary of the open volume at the stellar surface. Because the outer gaps are within the open volume, we divide the open volume into many parts, in which the shape of each part at the stellar surface is the same as the polar cap shape but the size is smaller. First we determine the coordinate values (x_0, y_0, z_0) of the last closed field lines at the stellar surface. Then the coordinate values (x_0', y_0', z_0') for different parts can be determined by using $x_0' = a_1x_0$, $y_0' = a_1y_0$ and $z_0' = (1 - (x_0'^2 + y_0'^2))^{1/2}$ and by changing a_1.

2.2 Pair production beyond the outergap boundary

Although pair production inside the gap is limited to a small region, pair production outside the gap is not the same case if synchrotron photons produced by secondary pairs exceed the thermal photons from the surface. The former photons do not get into the gap because of field line curvature (cf.CHR I) but they could convert most of the curvature photons from the gap into secondary pairs. We estimate the mean free path of curvature photon in the synchrotron X-ray photon field as follows: the γ-ray mean free path $\lambda_{{\rm X}\gamma} \approx (L_{\rm X}(2f_0)E_\gamma\sigma_{\rm p}/l^2\ c({\rm MeV})^2)^{-1} \approx 10^7(f_0/0.1)^{-1}L_{36}^{-1}l_8^2(E_\gamma/10{\rm GeV})^{-1}$ cm, where L_{36} is the X-ray luminosity in units of 10^{36} erg s^{-1}, l_8 is the characteristic length to the outer gap in units of 10^8 cm, E_γ is the typical energy of curvature radiation photons and $\sigma_{\rm p}$ is the pair production cross section. Here, we have considered that the threshold energy of pair production is $E_{\rm X}E_\gamma \geq ({\rm MeV})^2/(1-\cos\theta_{{\rm X}\gamma})$ and $\theta_{{\rm X}\gamma} \approx (2f_0)^{1/2}$. Since $l << R_{\rm L}$, so most curvature photons emitted from the accelerator will become secondary pairs outside the gap in some pulsars where the local magnetic field near the outer gap accelerator is sufficiently strong to give keV synchrotron radiation.

2.3 Photon emission morphologies

As pointed out above, in this model, two outer gaps can exist in the open field line volume of the pulsar magnetosphere (cf. Fig.1). Due to pair production, outer gaps are limited along

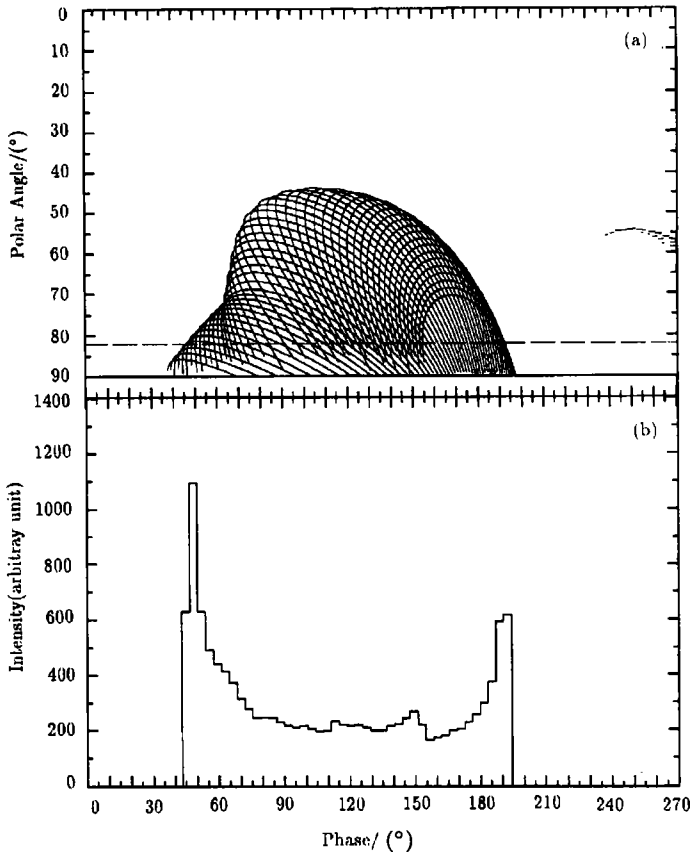

Fig 1. Emission projection onto the (ζ, Φ) plane and pulse profile. The emission consists of the emission outwards from both outer gaps and inwards only from the region $(r_{\rm lim} - r_{\rm in})$of both outer gaps. The outer gaps are limited along the azimuthal direction by pair production. (a) The emission projection ($a1 = 0.9$) and (b) corresponding pulse profile ($\Delta a1 = 0.03$). Crab parameters, $\alpha = 65°$, $\zeta = 82°$ and $\delta\phi = 160°$ are used.

both radial and the azimuthal directions. Therefore the model allows both outward and inward emission but inward emission is only from the region $(r_{\rm lim} - r_{\rm in})$ of the outer gaps. A large fraction of high energy photons emitted inwards cannot pass freely through the inner magnetosphere within a certain distance to the star where these photons are converted into secondary $e^{\pm}$ pairs by the intense magnetic field. These secondary pairs will emit lower energy photons through their synchrotron radiation. Part of that synchrotron photons will be further converted into pairs. Moreover, about half of the charged particles accelerated in the outer gap will move inwards along magnetic field lines. These charged particles will produce high energy curvature radiation photons. These curvature photons can be converted into pairs near the star. A cascade will develop there until the Lorentz factors of the pairs approach unity. Non-thermal X-rays can be produced in this cascade and thermal X-rays can be radiated from the stellar surface (Halpern & Ruderman 1993; Zhang & Cheng 1997; Cheng, Gil & Zhang 1998; Wang *et al* 1998; Cheng &

Zhang 1999).

2.4 Phase-resolved spectra

From the emission morphologies we see that photons emitted into a given phase come from different positions of the outergap. Fig. 4 shows the trajectory of the emission region for various pulsar phases for a given viewing angle. Since curvature radiation, synchrotron radiation and inverse Compton scattering depend on local quantities, e.g. curvature, $E_{||}$, B, $n_{\rm ph}$ etc., it is likely that the radiation spectrum varies with phase. First, the primary charged particles lose their energy via curvature radiation with a spectrum

$$\frac{{\rm d}^2\dot{N}_\gamma(r)}{{\rm d}V{\rm d}E_\gamma} = \frac{l_{\rm cur}(r)n_{\rm GJ}(r)}{E_{\rm cur}(r)}\frac{1}{E_\gamma} \quad {\rm for} E_\gamma \le E_{\rm cur}, \tag{9}$$

where $l_{\rm cur}(r) = {\rm e}E_{||}(r)c$ is the local power in curvature radiation produced by a single e^+/e^-, $n_{\rm GJ}$ is the local Goldreich-Julian number density and $E_{\rm cur}(r)$ is the local curvature radiation energy. In section 4, we pointed out that in many γ-ray pulsars most curvature photons will be converted into pairs by the synchrotron photons of the secondary pairs. The secondary pairs should then have the distribution

$$\frac{{\rm d}N_{\rm e^\pm}(r)}{{\rm d}E_{\rm e}} \approx \frac{1}{\dot{E}_{\rm e}}\frac{l_{\rm cur}(r)n_{\rm GJ}(r)}{E_{\rm cur}(r)}\ln\left(\frac{E_{\rm cur}}{E_{\rm e}}\right)\Delta V(r); \tag{10}$$

where $\dot{E}_{\rm e}$ is the rate of energy loss of the secondary pairs and $\Delta V(r)$ is the involved volume at position r. The radiation mechanisms of the secondary pairs include synchrotron radiation and inverse Compton scattering. The local pitch angle of the secondary pairs is approximated by $\sin\beta(r) \approx l(r)/s(r)$, where $l(r)$ and $s(r)$ are the local mean free path and the local radius of curvature respectively.

3 Applications

3.1 Crab pulsar

We apply this model to the Crab pulsar at first. In panel A of Fig. 3, the photon emission from a single outer gap in (ζ, Φ) plane is shown, where ζ is the polar angle from the rotation axis and Φ is the phase of rotation of the star. Part of the inward emission which can pass freely through the inner magnetosphere is also shown (dashed curves). The pulse profile corresponding to the emission pattern of panel A of Fig. 1 is shown in panel B of Fig. 1.

Fig. 2 are the comparisons between model results and the simultaneously observed data of OSSE, BASTE, COMPTEL and EGRET (Ulmer *et al.* 1995) for the Crab pulsar (Zhang, Cheng & Mei 2000).

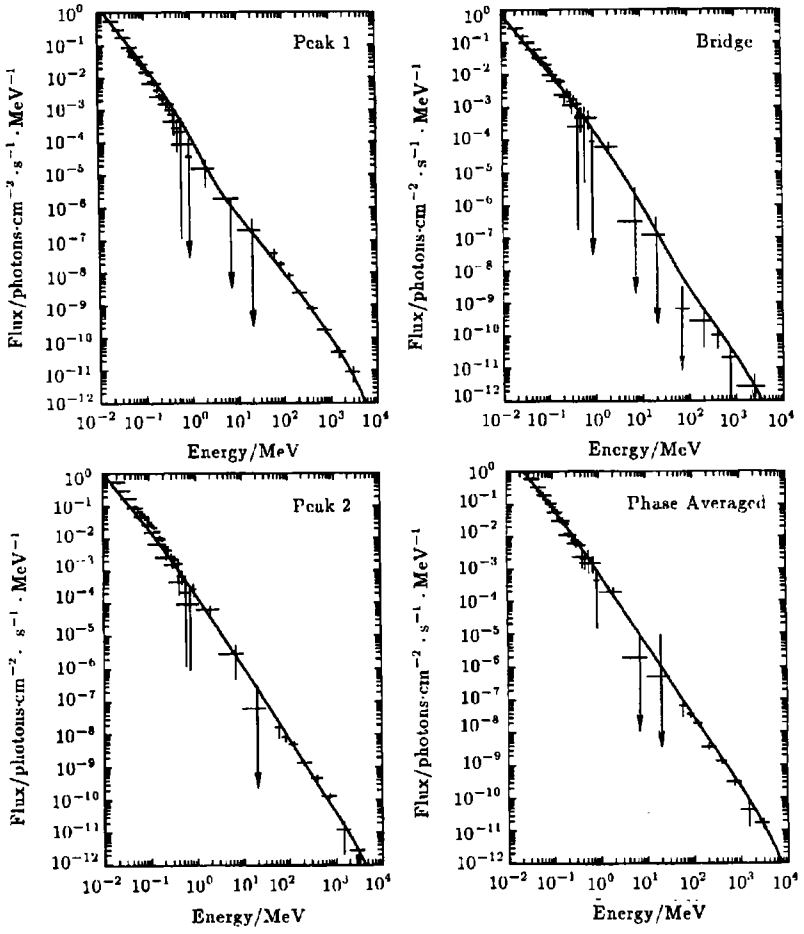

Fig. 2 The spectra of the Crab pulsar: peak 1, bridge, peak 2 and phase-averaged. Solid curves represents model results. The simultaneously observed data of OSSE BASTE, COMPTEL and EGRET are taken from Ulmer *et al.* (1995).

3.2 PSR B1509-58

PSR B1509-58 is believed to be a Crab-like pulsar because its parameter B/P^2 is very close to that of the Crab pulsar. PSR B1509-58 was discovered as an X-ray pulsar (Seward & Harnden, 1982). Its pulsed emission has been detected at radio frequencies (Manchester, Tuohy & D'Amico 1982), soft X-rays (Becker & Trümper 1997), hard X-rays (Kawai, Okayasu & Sekimoto, 1993; Matz *et al.* 1994; Rots *et al.* 1998), low energy γ-rays (e.g. Ulmer *et al.* 1993) and medium energy γ-rays (Carraminana *et al.* 1995, 1997; Kuiper *et al.* 1999). The observed data indicate that (i) the light curves of hard X-rays and low energy γ-rays have broad single peak, (ii) the X-ray pulse lags the radio by about 0.27 ± 0.01 period, with no evidence for any energy dependence in the range $2 \sim 100$ keV (Rots *et al.* 1998), (iii) low energy γ-ray pulse lags the radio by 0.32 ± 0.02 (Ulmer *et al.* 1993) or ≈ 0.3 (Rots *et al.* 1998), and (iv) medium energy γ-ray pulse lags the radio by 0.30 ± 0.06 (Carraminana *et al.* 1997). Rots *et al.* (1998) pointed out that the change in phase lags of X-rays and low energy γ-rays would be due to a gradual change in dispersion

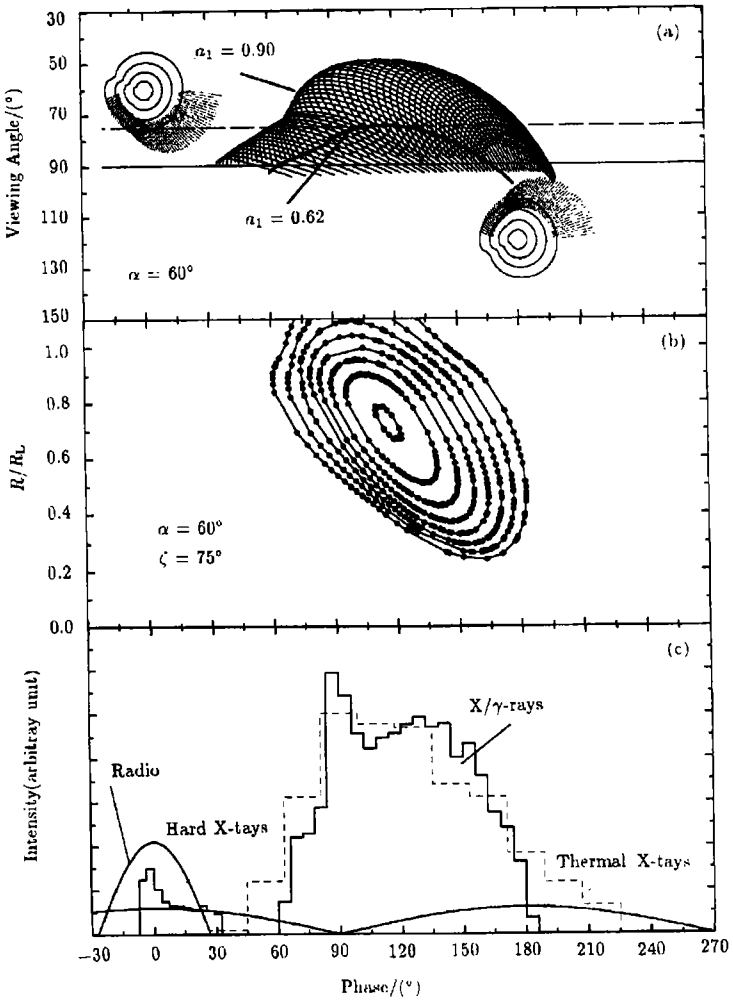

Fig. 3 Emission projection onto the (ζ, Φ) plane and pulse profile for PSR B1509-58 ($\alpha = 60°$). Panel A: Photon emission from the pulsar as a function of phase, the solid curves indicate outward photon emission from the emission region above a single outer gap. The tiny-dashed curves represents inward and outward non-thermal photon emission from the region near the stellar surface. The observed lines of sight at $\zeta = 75°$ and $\zeta = 90°$ (dashed and solid lines), and both polar caps (contours) are shown. Panel B: The variation of radial distance with pulse phase for the thickness of the emission region of $\approx 0.11 R_{\rm L}$. The curves represent trajectories for $a_1 = 0.90$, 0.86, 0.82, 0.78, 0.74, 0.70, 0.66 and 0.62. Panel C: Pulse profile for PSR B1509-58. The model X-ray/γ-ray pulse at $\zeta = 75°$ is shown.

measure. According to the thick outer gap model, hard X-rays and low energy γ-rays have the same origin, i.e. they are produced by synchrotron self-Compton radiation of secondary $e^{\pm}$ pairs of the outer gap. Therefore, the phase offsets of hard X-rays and low energy X-rays with respect to the radio pulse are the same. However, a small phase lags between X-rays and low energy γ-rays are still possible because the emission regions of X-rays and γ-rays are very thick. Each

layer of the emission can contribute to X-rays and γ-rays differently. For example, synchrotron radiation from the regions near light cylinder radius contribute less gamma-ray than the regions near the star.

The light curve and spectra of PSR B1509-58 can be explained in terms of the three dimensional outer gap model described in section 3.2. In order to determine the emission pattern, we need to know the magnetic inclination angle and viewing angle. Unfortunately, we cannot get any constraints on two angles from radio observation. However, these two angles can be estimated because of the following constraints: (i) viewing angle must cross the radio beam which is $\approx 6.3/\sqrt{P} \approx 16.3°$ for PSR B1509-58 and (ii) the phase offset with respect to radio pulse is ≈ 0.3 and the pulse is a single broad peak. It turns out that the model light curve with a magnetic inclination angle of about 60° and a viewing angle of 75° can compare with the observed light curves (Zhang and Cheng. 2000). After determining the inclination and viewing angles, one can follow the calculation procedure described above to determine the emission patterns. The emission patterns are shown in panel A of Fig. 3. Using equation (5), the fractional size of the outer gap is $f_0 \approx 0.12$. Such thickness cannot use only one representative surface to calculate the high energy spectra. In panel B of Fig.3, eight surfaces are used and the light curves for various wavebands are shown in the panel C of Fig.3. The model phase-average spectra is compared with the observed data shown in Fig.4. Here, the observed pulse profile data for the X-ray band of $16 \sim 32$ keV were measured by RXTE (Rots *et al.* 1998).

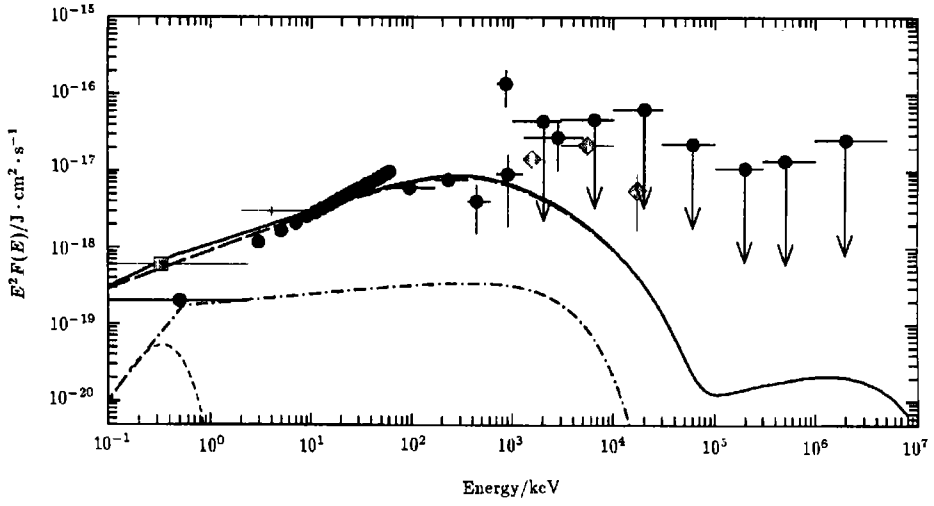

Fig. 4 The comparison of model spectra with the observed data for PSR B1509-58. The solid curve represents model result for $\sin(\beta(R_L))$ =0.5. We have used the observed data compiled by Thompson *et al.* (1999), ROSAT data (box) (Becker & Trümper 1997), ASCA data (cross) (Saito 1998) and COMPTEL data (solid diamonds) (Kuiper *et al.* 1999).

Although the phase-resolved spectra of PSR B1509-58 are not known, Zhang and Cheng (2000) calculate the radiation spectrum from PSR B1509-58 by dividing the phase into three bins: $\approx -15° \leq \phi \leq \approx 50°$, $\approx 60° \leq \phi \leq \approx 180°$, and $\approx 180° \leq \phi \leq \approx 270°$(cf. Panel C of Fig. 3).

In the phase bin from 180° to 270°, the photon emission is dominated by thermal photons coming from the stellar surface, and the expected thermal photon spectrum is shown in Fig.4, where the isotropic emission is assumed. The spectrum of the non-thermal photons in the phase bin from $\approx -15°$ to 50° is shown in Fig.4, where the photons are produced near the stellar surface due to the cascade process and the beaming solid angle is assumed to be 1 sr. The non-thermal photon emission above the outer gap ranges from $\approx 60°$ to $\approx 180°$.

3.3 PSR B0540-69

PSR B0540-69 was discovered in the soft X-ray band by Einstein X-ray Observatory (Seward, Harnden & Helfand, 1984). Optical and radio pulses were detected by Middleditch & Pennypacker (1985) and Manchester *et al.* (1993) respectively. Moreover, X-ray pulses from PSR B0540-69 have been detected by various X-ray detectors such as GINGA (Nagase *et al.* 1990; Deeter, Nagase & Boynton 1999), ROSAT (Finley *et al.* 1993; Eikenberry, Fazio & Ransom 1998), BeppoSAX (Mineo *et al.* 1999),and Chandra (Gotthelf & Wang 2000), but the pulses of γ-rays have not been detected by OSSE, COMPTEL and EGRET and only upper limits in those energy ranges are available. All these observations indicate that (i) PSR B0540-69 has a single broad pulse profile at radio band, (ii) there is a close alignment between optical and X-ray pulse profiles. Although radio pulse has been detected, the pulse offset of X-ray with respect to radio pulse has not been known.

PSR B0540-69 is one of the youngest rotation-powered pulsars. Its energetic behavior and age have been noted as similar to those of the Crab pulsar, but pulse profiles are different. In fact, X-ray/γ-ray emission from the Crab pulsar indicate two peaks with phase separation ≈ 0.4. Following the similar calculation procedure as described for PSR B1509-58, The light curves, emission pattern and spectra of PSR B0540-69 are shown in Fig.5 and Fig.6.

Again the phase-resolved spectra of PSR B0540-69 are divided into three phase bins: $\approx -15° \leq \phi \leq \approx 50°$, $\approx 60° \leq \phi \leq \approx 180°$, and $\approx 180° \leq \phi \leq \approx 270°$. In the phase bin from 180° to 270°, the photon emission is dominated by thermal photons coming from the stellar surface(see Fig.5). In the phase bin from $\approx -15°$ to 50°, the photon emission is dominated by the non-thermal photon spectrum produced near the stellar surface due to the cascade process. One can see that the thermal component is negligible compared the non-thermal component. In the phase bin from $\approx 60°$ to $\approx 180°$, the phase-resolved spectrum is dominated by the non-thermal photon emission above the outer gap (see Fig.6). It can be seen that this photon emission is from optical to γ-ray ranges. Observed data at optical waveband are taken from Middleditch *et al.* (1987), Hill *et al.* (1997). The data at ROSAT energy range, BeppoSAX energy range, COMPTEL and EGRET are taken from Finley *et al.* (1993), Mineo *et al.* (1999), Hermsen *et al.* (1994) and Thompson *et al.* (1994) respectively.

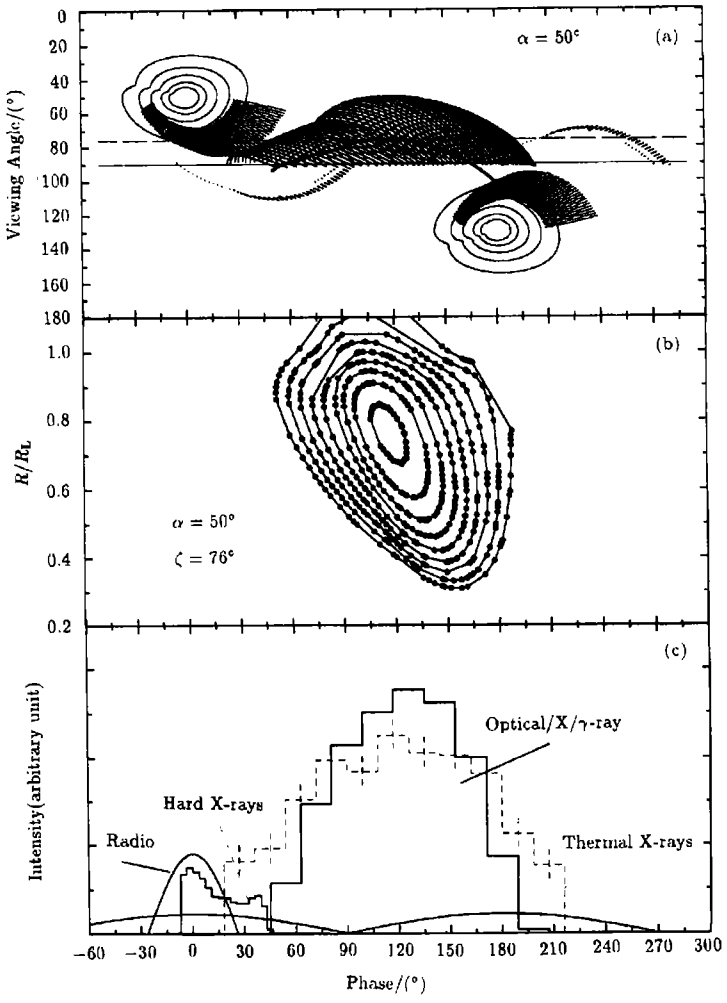

Fig. 5 Emission projection onto the (ζ, Φ) plane and pulse profile for PSR B0540-69 ($\alpha = 50°$). Panel A: Photon emission from the pulsar as a function of phase. The solid and dashed curves indicate inward and outward photon emission from the finite region above a single outer gap respectively. The tiny-dashed curves represents inward and outward non-thermal photon emission from the region near the stellar surface. The observed lines of sight at $\zeta = 70.5°$ and $\zeta = 90°$ (dashed and solid lines), and both polar caps (contours) are shown. Panel B: The variation of radial distance with pulse phase for the thickness of the emission region of $\approx 0.08R_{\rm L}$. The curves represent trajectories for $a_1 = 0.93$, 0.91, 0.89, 0.87, 0.85, 0.83, 0.81 and 0.79 respectively. Panel C: Pulse profile for PSR B0540-69. The model optical/X-ray/γ-ray pulse at $\zeta = 70.5°$ is shown.

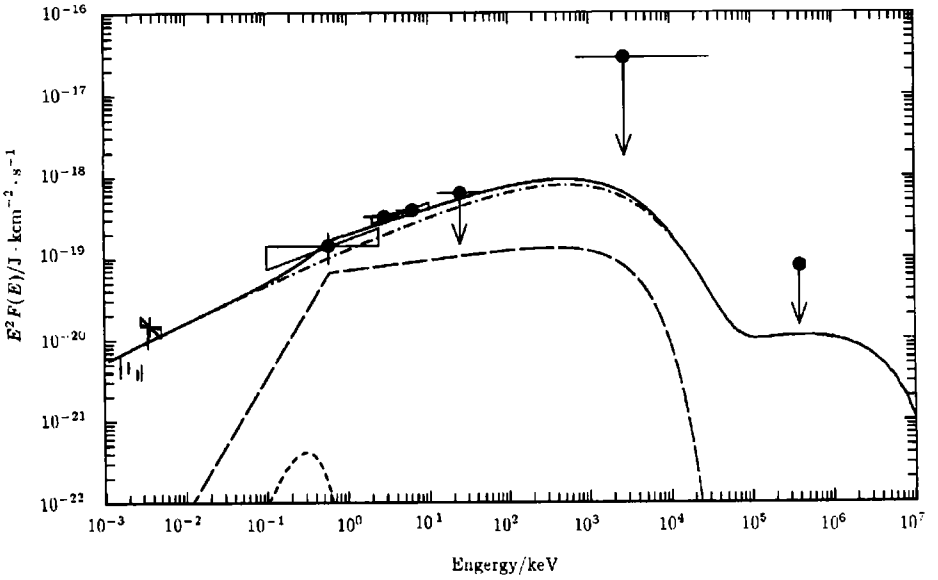

Fig. 6 The comparison of predicted phase-averaged spectrum with the observed data for PSR B0540-69. Observed data at optical waveband are taken from Middleditch *et al.* (1987), Hill *et al.* (1997). The data at ROSAT energy range, BeppoSAX energy range, COMPTEL and EGRET are taken from Finley *et al.* (1993), Mineo *et al.* (1999), Hermsen *et al.* (1994) and Thompson *et al.* (1994) respectively. The solid curve represents phase-averaged spectrum for $\sin(\beta(R_{\rm L})) = 0.25$. The dot-dashed, long-dashed and short-dashed curves represent photon spectra in different phases.

4 Summary

We use a 3-D model magnetosphere to give the observed light curve and the phase-resolved spectra of the γ-ray pulsars. In our model, the local photon-photon pair production in the outer gaps limits the extension of the outer gaps along the azimuthal direction. We find that the two topological disconnected outer gaps, with some extension along the azimuthal (ϕ) direction, exist in the pulsar magnetosphere. Double-peaked pulse profiles and single pulse profiles with varying phase separation depend on viewing angle and inclination angle. For the Crab pulsar, a double-peaked pulse profile with a strong bridge emission occur naturally, as in the single pole outer gap model. Although pair production inside the outer gap is only limited to a small region, the intense X-rays produced by secondary pairs in the outer-magnetosphere of the Crab pulsar can convert most curvature photons into pairs outside the gap. However, for the PSR B1509-58 and PSR B0540-69, single pulse profiles are observed in the X-ray bands. According to our model, we expect that the γ-ray pulse profles from these two pulsars have also single pulse profiles.

Acknowledgements We thank R.W. Romani for useful discussion and suggestions, and M.P. Ulmer for OSSE, BASTE and COMPTEL data of the Crab pulsar. This work is partially sup-

ported by an RGC grant of the Hong Kong Government and National Nature Science Foundation of China.

References

Becker W, Trümper J. 1997, Astron. Astrophys., 326: 682
Carraminana A, Bennett K, Buccheri R *et al.* 1995, Astron. Astrophys. 304: 258
Carraminana A, Bennett K, Hermsen W *et al.* 1997, In: Dermer C D. Strickman M S, Kurfess J D eds. AIP Conf. Proc. 410. Proceedings of the Fourth Compton Symposium, New York: AIP, 583
Cheng A F, Ruderman M A, Sutherland P G. 1976, Ap. J., 203: 209
Cheng K S, Ho C, Ruderman M A. 1986a, Ap. J., 300, 500 (CHR I)
Cheng K S, Ho C, Ruderman M A. 1986b, Ap. J., 300, 522 (CHR II)
Cheng K S, Gil J, Zhang L. 1998, Ap. J., 493, L35
Cheng K S, Ruderman M, Zhang L. 2000, Ap. J., 537, 964
Cheng K S, Zhang L. 1999, Ap. J., 515, 337
Chiang J, Romani R W. 1992, Ap. J., 400, 724
Chiang J, Romani R W. 1994, Ap. J., 436, 754
Deeter J E, Nagase F, Boynton P E. 1999, Ap. J., 512, 300
Eikenberry S S, Fazio G G, Ransom S M. 1998, Ap. J., 492, 754
Fierro J M. 1995, Ph. D. Thesis, Stanford University
Fierro J M, Michelson M, Nolan P L *et al.* 1998, Ap. J., 494: 734
Finley J P, Ögelman H, Hasinger G *et al.* 1993, Ap. J., 410, 323
Gotthelf E V, Wang Q D. 2000, Ap. J., 532: L117
Halpern J P, Ruderman M. 1993, Ap. J., 415: 286
Hermsen W *et al.* 1994, Ap. J., 92: 559
Hill R J, Dolan J F, Bless P T *et al.* 1997, Ap. J., 486: L99
Holloway N J. 1973, Nature Physical Science, 246: 6
Kawai N, Okayasu R, Sekimoto Y. 1993, In: Friedlander M, Gehrels N, Macomb D J. ed. AIP Conf. Proc. 280, Compton Gamma-Ray Observatory, New York: AIP, 204
Kuiper L, Hermsen W, Krijger J M *et al.* 1999, Astron. Astrophys., 351: 119
Manchester R N, Tuohy I R, D'Amico N. 1982, Ap. J., 262: L31
Manchester R N, Mar D P, Lyne A G *et al.* 1993, Ap. J., 403: L29
Matz S M, Ulmer M P, Grabelsky D A *et al.* 1994, Ap. J., 434: 288
Middleditch J, Pennypacker C R, Burns M S. 1987, Ap. J., 315: 142
Mineo T, Cusumano G, Massaro E *et al.* 1999, Astron. Astrophys., 348: 519
Nagase F, Deeter J, Lewis W *et al.* 1990, Ap. J., 351: L13
Rots A H, Jahoda K, Macomb D J *et al.* 1998, Ap. J., 501: 749
Romani R W. 1996, Ap. J., 470: 469
Romani R W, Yadigaroglu I A. 1995, Ap. J., 438: 314
Saito Y. 1998, Ph.D thesis
Seward F D, Harnden F R. 1982, Ap. J., 256: L45
Seward F D, Harnden F R, Helfand D J. 1984, Ap. J., 287: L19
Thompson D J *et al.* 1996, Ap. J., 465: 385
Ulmer M P, Matz S M, Grabelsky D A *et al.* 1995, Ap. J., 448: 356
Thompson D J, Arzoumanian Z, Bertsch D L *et al.* 1994, Ap. J., 436: 229
Wang F Y-H, Ruderman M, Halpern J P *et al.* 1998, Ap. J., 498: 373
Zhang L, Cheng K S. 1997, Ap. J., 487: 370
Zhang L, Cheng K S, Mei D C. 2000, Chin. Phys. Lett., 17: 544
Zhang L, Cheng K S. 2000, Astron. Astrophys., 363: 575